33RD CONGRESS
OF THE INTERNATIONAL COUNCIL
OF THE AERONAUTICAL SCIENCES
STOCKHOLM, SWEDEN, 4-9 SEPTEMBER, 2022

ICAS 2022 SWEDEN

A COMPARATIVE ANALYSIS OF INNOVATIVE DIGITAL HYDRAULIC ACTUATORS FOR PRIMARY FLIGHT CONTROL

Rodrigo Simoes Lopes Junior[1], Dimitri Oliveira e Silva[1], Marcos Paulo Nostrani[1], Alessandro Dell'Amico[2], Petter Krus[3] & Victor Juliano De Negri[1]

[1]Laboratory of Hydraulic and Pneumatic Systems (LASHIP), Federal University of Santa Catarina (UFSC), Brazil
[2]Saab AB, Linkoping University (LiU), Sweden
[3]Division of Fluid and Mechatronic Systems (FLUMES), Linkoping University (LiU), Sweden

Abstract

The primary flight control surfaces are essential to keep the aircraft flying in safety conditions during the entire flight (take off, cruise and approach). These surfaces are normally controlled by hydraulic actuators, especially the servo-hydraulic actuators, which are known by their low energy efficiency caused by the throttle losses and leakage. In this paper, new topologies of hydraulic flight control actuators using digital hydraulics are presented and discussed from the perspectives of the system control and energy efficiency. In order to evaluate the improvements in energy efficiency, dynamic simulations were carried out in a delta-canard aircraft model, which was integrated with the digital hydraulic actuators to control the aircraft elevons in different missions within distinguished points of its operational envelope. Comparing the digital topologies with the well-established servo-hydraulic actuator used as a benchmark model, the results shown an increased energy efficiency from 3 to 90 times under the studied flight missions.

Keywords: Flight Control Actuators, Digital Hydraulics, Efficient Actuators, Dynamic Simulation

1. Introduction

The unique properties of hydraulic systems, such as high power density and stiffness, fast dynamic response and constructive simplicity, have made them the most used solution in aircraft systems [1]. Although some advantages have emerged with the new trend of More Electric Aircrafts (MEA), they are still considered the most reliable solution for flight control actuators [2] [3]. However, the servo-hydraulic actuators (SHA), which are known as the typical solution for flight control systems (FCS), present low energy efficiency, caused mainly by the throttle control techniques and internal leakages presented in the servovalves (SV) [4]. These facts have motivated the development of more efficient solutions, where the digital hydraulic systems stand out as an attractive alternative combining reliability, performance and energy savings, due to the reduction of the throttle losses [5].

In this context, the bilateral Brazil-Sweden collaboration between LASHIP-UFSC, FLUMES-LiU, CERTI, and Saab AB has shown promising results with new actuator designs for primary control surfaces based on innovative digital hydraulic topologies. During the last decade, the research team has thoroughly investigated three main topologies of digital control actuators, which are distinguished by the use of different hydraulic power supply systems, control strategies and system architectures, resulting in fly-by-wire (FBW) or power-by-wire (PBW) concepts.

Studies using mathematical models, dynamic simulations, and a digital hydraulic test rig installed at LASHIP have shown a significant reduction in energy dissipation with consequent improvement of the efficiency levels by using the digital hydraulic approaches. One of the digital hydraulic actuator topologies, presented in [6] and [7], is named Digital Hydraulic Actuator (DHA), which is based on the FBW concept. In this case, the results showed an increase in the system efficiency levels up to 29 times when compared to an SHA working in the same conditions.

Another actuator topology denominated Digital Electro-Hydrostatic Actuator (DEHA) [8] was proposed, which uses the PBW principle, presented an increase in the efficiency levels around 31 times in a comparison with the same SHA used in [6] and [7]. In addition, a new topology that is also

a PBW design, is the Variable Motor Digital Electro-Hydrostatic Actuator (VMDEHA) [9]. It includes aspects of the Electro-Hydrostatic Actuator (EHA) and the DEHA, however, a new control strategy based on optimal efficiency operating points of its digital pump and variable speed electric motor are implemented [10].

Nevertheless, in order to increase the readiness level of the proposed technologies, a deep investigation of the use coupled to aircraft primary control surfaces is mandatory, especially considering the interactions between the discrete behavior of digital actuators, the aircraft dynamics and the FCS. Therefore, the aircraft model Aero-Data Model in a Research Environment (ADMIRE) [11] has been used by the research team for the evaluation of the proposed actuators. In [12], a hybrid solution for the ADMIRE aircraft using the DHA for the inner elevons and the SHA for the other flight control surfaces was proposed. The results shown that is possible to achieve an input energy-saving around of 20% just replacing two of the six proportional actuators for the digital ones. Recently, a new study considering all the ADMIRE elevons controlled by a DHA model with improved parameters was carried out, where the dynamic behavior of all actuators and aircraft in a flight mission close to the aircraft operational envelope limits were investigated. As a result, the proposed DHA increased the energy efficiency levels around 28 times compared with the equivalent SHA, leading a reduction in the input energy levels around 18 times in the aircraft model with all elevons controlled by DHA, without significantly affecting the aircraft flight stability [13].

Therefore, in order to go forward in the energy efficiency and performance analysis of digital hydraulic solutions for primary flight control surfaces, this paper presents the main aspects of the three proposed actuator topologies and a comparative analysis of their use to control the ADMIRE aircraft elevons.

This paper is organized as follow. In Section 2, a bibliography analysis of the main requirements for primary flight control actuators of current aircrafts in order to provide baseline values for the sizing process is presented. In Section 3, the proposed digital hydraulic topologies are presented considering their particularities, such as their components and subsystems, integration in the aircraft system, and control principles. Also in Section 3, a re-parametrization of the validated models, for the ADMIRE aircraft, is shown. Section 4 presents the main simulation results for different flight missions and aircraft flight qualities parameters comparing with the typical SHA.

2. Review of Primary Flight Control Design and Baseline Systems

2.1 Design of primary flight control actuators

According to [14] and [15], the United States Air Force (USAF) standard MIL-F-8785C [16] has been the most used reference document to obtain quantitative performance criteria for military piloted aircraft. This standard presents a vast and detailed set of requirements that must be followed in order to ensure adequate levels of flight and handling qualities, regardless of the implementation or mechanization of the aircraft. In the same way, the standard USAF MIL-F-9490 [17], which comprises a series of criteria for general performance, design development and quality assurance requirements for the FCS of USAF aircrafts, has aided engineering specialists in preliminary design of future aircraft and FCS components [18].

However, the main challenge for designing actuators for flight control surfaces is that neither the standards nor the reference documents describe how to define the static and dynamic performance requirements of these systems. It is known that characteristics such that time or frequency responses, position errors, magnitude and dynamics of disturbance forces, etc. are very sensitive for the aeronautical industry companies and, consequently, the design at lower TRLs must consider some approximated values. Nevertheless, as a starting point for the development of new primary actuators proposals, comparative analysis using aircraft and actuator models and experimental data from proof-of-concepts is a convenient approach for investigating the proposed designs. The dynamic and static properties of the actuators and their impact on the flying and handling qualities allows the preliminary definition of minimum acceptable limits of the systems under development [19].

According [20], the requirements imposed for primary flight control surface actuators are very restrict, such as the ability to operate with displacements below 1% of their total stroke. In general, they must be able to reach the flight surface angle required by the FCS with restrict levels of accuracy and

stability, and with low response time. In addition, they must to be able to reject disturbances from aerodynamic forces variations [21]. Therefore, a first step in the design process of flight control actuators is to determine which parameters must be considered. In the case of hydraulic actuators, the basic design parameters are [22]:

- The pressure values of the supply and return lines (p_s and p_T);
- The maximum hinge moment of the flight surface ($H_{m,\,max}$);
- The maximum deflection required by the flight surface (δ_{max});
- The maximum deflection rate in a no-load condition of the flight surface ($\dot{\delta}_{max}$);
- The steady-state gain between the actuator and the flight surface (K_δ) (lever ratio);
- The flight surface inertia moment (J);
- Control surface natural frequency (Control surface flutter suppression required by the hydraulic actuator) (ω_n);
- The damping coefficient of actuator/flight surface system (ξ).

As stated by [23] and [24], in regular conditions, most of flight control actuators operate below the maximum designed workload. For example, [24] shows the aileron operating ranges for an Airbus A320, where from -80% to 20% of the available force capacity and 15% of their maximum speed are used. In addition, the typical ranges of required force in a military combat aircraft versus a civilian transport aircraft are presented in [2]. The results show that the values can achieve 5% to 40% for the landing and take-off, 5% to 20% in the cruise, and 60% to 100% in turbulent flight or combat, considering the maximum available force.

Therefore, to properly develop an aircraft FCS, recognizing the static and dynamic properties of the flight control actuators is critical because of their direct relationship to the aircraft flying and handling qualities. In this context, to provide reference values for a preliminary design of flight control surface actuator, Table 1 presents the main performance requirements identified in the literature related to some aircrafts.

Table 1 – Performance requirements for flight control surfaces*

Aircraft		Airbus A320	Boieng 767	Lockheed C-141	NASA F-18 SRA	General Dynamics F-16	NASA Hyper X43A	Aermacchi M346	Prototype USAF
Flight Surface		Aileron	Aileron	Aileron	Flaperon	Rudder	Rudder	Aileron	Generic
Actuator		SHA	SHA	SHA	EHA	SHA	EMA	SHA	EMA
Stroke	mm	44		85/-52	114		66	65	
	°		±25	-		±30			±30
Velocity	mm/s	90		118	195		88,9	≈ 180	
	°/s		55			120			80
Maximum Workload	kN	48		85	59		11,12	65	
	kNm		8,6			6,5			4,2
Bandwith	Hz	≈ 1	≈ 3	4	7	3,8	7,5	4	8
Stifness	kN/mm	-	-	105	50		70	80	
	kNm/rad					290			300

* Presented in [19], based on [24]–[33].

2.2 Design constraints for the ADMIRE elevons

The aircraft model used in this paper is the ADMIRE. This simulation software implements a Generic Aerodata Model of an unstable aircraft (GAM) with 6 degrees of freedom in a delta canard single-seat configuration, including models of FCS, engine, actuators, and sensors [11]. The GAM was developed by Saab AB and KTH in 1996 and, since then, has been improved and used as a complete aircraft model, supporting several studies in aircraft modeling and design of the control systems with aerodynamic data [11] [34].

2.2.1 ADMIRE original actuator models

As the focus of this section is to discuss the constraints that were made to define the design requirements for the ADMIRE elevons, the structure of the models for flight control actuators that are presented in ADMIRE are discussed. All the ADMIRE control surface actuators (rudder, canards, inner and outer elevons) are modeled with the same structure presented in the block diagram shown in Figure 1.

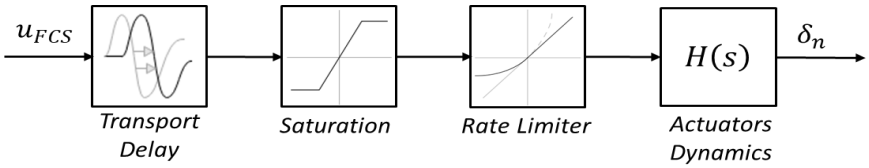

Figure 1 - ADMIRE actuator block diagram.

The signals from the ADMIRE FCS (u_{FCS} [rad]) are used as a reference for the angular position for the actuator models and the transport delay of 20 ms is used to simulate the effect of the FCS computers. The saturation block limits the maximum and minimum positions of the actuators, which are presented in [11]. The rate limiter function is added to limit the maximum speed of the actuators, since fast movements should be avoided to prevent the flutter effect or conflicts with the aircraft FCS. In this case, the maximum angular velocity is 0.87 rad/s. The dynamics of the actuators are modeled as a first-order linear system H(s) with a time constant τ equals to 0.05 s. This function provides the deflection of the control surfaces (δ [rad]) for the GAM.

The hinge moment (H_m) imposed by the aerodynamic forces in the flight control surfaces is estimated by a subroutine available in ADMIRE, being expressed by

$$H_m = \bar{q}.S_e.c_e.C_{HFs}, \tag{1}$$

where, $\bar{q}$ [Pa] is the dynamic pressure caused by the airflow in the control surface, S_e [m] and c_e [m] are the control surface flat area and the mean aerodynamic chord, respectively. The C_{HFs} is the aerodynamic hinge moment coefficient, which is a function of the aircraft states [14].

2.2.2 Design requirements for the hydraulic actuators

From the analysis of the ADMIRE model (Section 2.2.1), it is clear the problem with defining the design requirements for any new actuator requires the knowledge of dynamic parameters and workload levels. As the proposed actuators are linear, a length lever that results on adequate steady-state flight surface deflection rate (K_δ), must be defined. Therefore, the relation between the linear and rotational movements are defined by

$$\Delta x_{ac} = l_{K_\delta}.\sin\delta, \tag{2}$$

and

$$F_{ext} = \frac{H_m}{l_{K_\delta}\cos\delta}. \tag{3}$$

The angular displacement δ [rad] is converted into linear displacement Δx_{ac} [m] and the flight surface aerodynamic moment H_m [N.m] is converted into an external force F_{ext} [N], being both functions inputs for the model of the actuators. The inverse function is used to convert the linear motion of the actuators in rotational motion, which are sent to the GAM. The lever length $l_{k\delta}$ was defined as 0.1 m, based on the maximum linear displacement of 0,05 m that the actuator must produce in order to achieve the

maximum angular displacement of the ADMIRE elevons of ±30°.

Considering the presence of the rate limiter (Figure 1), the maximum angular rate of 0.87 rad/s was used to determine the maximum velocity v_{max} of the actuators, resulting in 0.1 m/s. A second-order transfer function was used to describe the response for the hydraulic actuators, such that the expected bandwidth ω_n [rad/s], for the proposed actuators, can be defined according to [35], being

$$\omega_n = \frac{v_{max}}{x_{st}.0.37}, \tag{4}$$

where x_{st} [m] is the desired steady-state displacement, being for the proposed actuators a half of the maximum actuator displacement (Δx_{ac}).

With these parameters, the resulting bandwidth is equal to 10.81 rad/s, leading a settling time of 0.53 s, considering an underdamped system with a 0.9 damping ratio (ξ). However, the bandwidth calculated from Equation (4) represents a minimum value for an adequate dynamic response. For this work, it was considered as 12.56 rad/s (2 Hz).

Based on Equation (1) and in simulations for the valid ADMIRE FCS envelope [11], the maximum load t of 100 kN for the actuators was determined. This value was estimated considering the maximum hinge moment in the GAM elevons. As a result, the maximum hinge moment for the elevons is limited to a range between 10 kNm and 8.66 kNm at 0° and 30°, respectively. The maximum system pressure and the reservoir pressure were specified as 280 bar and 7.5 bar, respectively, based on typical values for aircraft hydraulic systems.

For all actuators, the same inertia and friction parameters were considered. The friction was modeled according to the LuGre model, and the parameters that were considered are described in [13]. Table 2 presents the main design requirements used for the sizing of the proposed hydraulic actuators.

Table 2 – Hydraulic actuator design requirements for ADMIRE elevons.

Parameters	Symbol	Value	Unit
Maximum speed	v_{max}	0.1	m/s
System bandwidth	ω_n	12.56	rad/s
Inertia load	M_t	300	kg
Steady-state displacement	x_{st}	0.025	m
Supply pressure	p_{sup}	280	bar
Reservoir pressure	p_{res}	7.5	bar
Maximum external load	F_{MAX}	100	kN
Viscous Friction	B_t	5×10^4	Ns/m
Lever length	l_{lever}	0.1	m
Bulk modulus	β	1.3×10^9	Pa
Fluid density	ρ	850	kg/m³

2.3 Base line system description

As a baseline system, the same tandem duplex SHA model presented in [13] was used (Figure 2a). In this system, two servovalves (SV) control the cylinder simultaneously, where each one is responsible for 50% of the total load. Therefore, the size of the areas were calculated considering the maximum external load requirement (F_{MAX} = 100 kN), and the load pressure p_c equal to two-thirds of the supply pressure p_{sup}([35]), resulting in 0.0027 m².

The SV model was developed by [7] and comprises the parameters identified by experimental tests using SV MOOG model 760 C263-A (Table 3), where its total internal leakage was identified. The leakage is associated with the pilot stage and the clearances of the SV and has the maximum value in the valve null position (≈ 1.8 L/min at a pressure differential of 210 bar) and decreases with the valve opening, assuming a constant value above ±3V (≈ 0.8 L/min at a pressure differential of 210 bar). As a result, the hydraulic power unit must provide a minimum flow rate to keep the system pressurized, which results in low energy efficiency when it operates at small valve spool displacements.

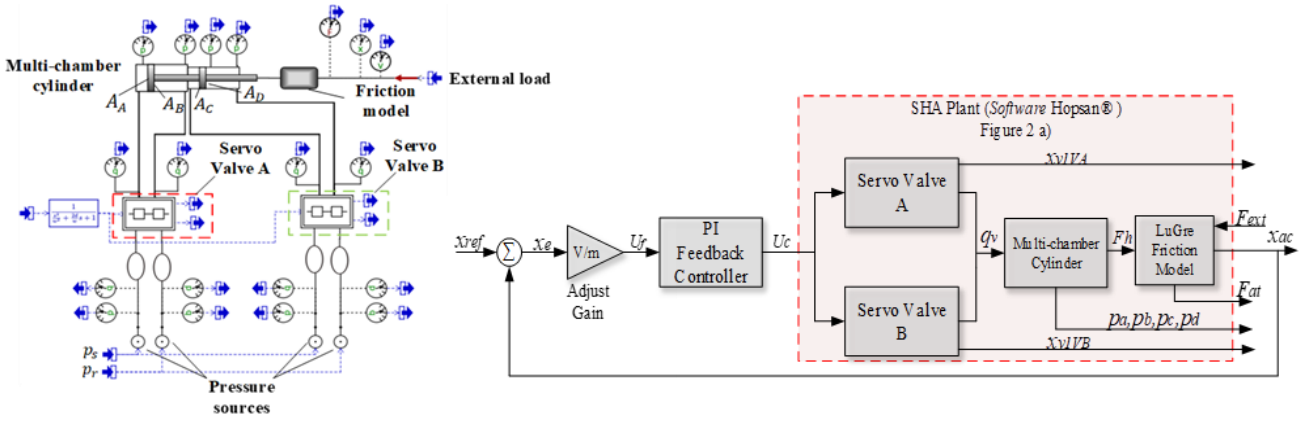

a) b)

Figure 2 - SHA used as a benchmark system: a) Hopsan model; b) System block diagram.

Table 3 – SV parameters [7].

Parameter	Symbol	Value	Unit
Configuration	-	4/3 closed center	-
Nominal flow rate	q_{vn}	3.15×10^{-4} @ 210 bar	m³/s
Flow coefficient	k_v	1.2×10^{-7}	$m^3/sPa^{1/2}$
Control signal	U_c	±10	V
Bandwidth	ω_{SV}	1256.64	rad/s
Damping ratio	ξ_{SV}	0.9	-

Considering the design requirement for the flight surface of ≈ 12.56 rad/s, the bandwidth for the servovalve of the SHA must be at least 5 times higher than the system bandwidth (≥ 62.8 rad/s) [35]. In this case, by the presented data from Table 3, the proposed SV achieves the dynamic requirement. The flow coefficient of a symmetrical 4-way SV is defined by [35]

$$k_v = \frac{q_{vc,max}}{\sqrt{p_s - |p_c|}}. \quad (5)$$

For attending the system requirements, Equation (5) results on a k_v of 0.398×10^{-7} $m^3/sPa^{1/2}$. Therefore, the SV described in Table 3 can be used.

In the proposed SHA control system (Figure 2b), the PI controller is used with fixed gains and a closed loop based on the cylinder position Δx_{ac} feedback. The proportional and integral gains were set as 5 and 1, respectively. A constant of 400 V/m was used to convert the position error to the SV control signal.

3. Proposed Digital Hydraulic Topologies

The digital hydraulic actuators discussed in this paper use a set of on/off valves associated with a multi-chamber cylinder. However, they differ by the arrangement of the valves, power unit, operating principle, and control strategy. Using the Hopsan software [36], all the models were developed and incorporated into the ADMIRE elevons to evaluate the behavior of the actuators and the aircraft. In the following sections, the proposed digital hydraulic actuator topologies will be presented and their characteristics will be discussed.

3.1 Digital Hydraulic Actuator – DHA

The first topology proposed as an actuator solution for primary flight control surface is called Digital Hydraulic Actuator (DHA) (Figure 3), which was developed by [2] and results discussing its potential to save energy in aircraft systems presented in [6], [12] and [13]. Furthermore, additional studies were carried out focused on improving the control system, failure modes and system reliability [19], [37].

Based on a secondary control design, the DHA comprises a multi-chamber cylinder and constant supply pressure lines, which are connected to the chambers of the cylinder by on/off valves.

Consequently, the DHA input energy is provided by different hydraulic pressure supply lines. The DHA uses 3 ideal pressure lines with different pressure levels, a multi-chamber cylinder with 4 different areas, and 12 on/off valves to supply each pressure line to each chamber, resulting in 81 discrete forces levels (Figure 4a).

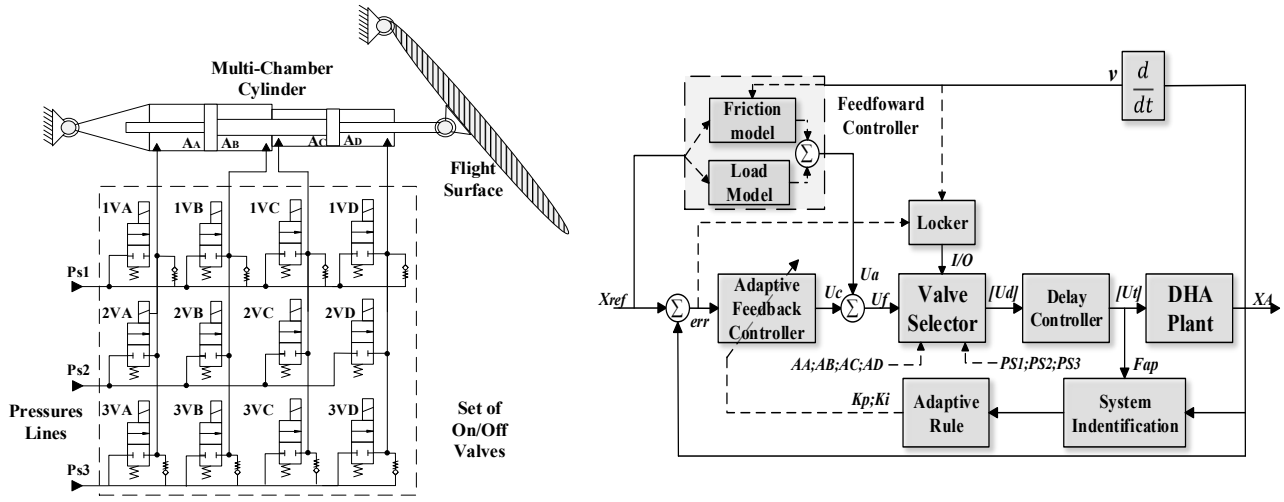

a) b)

Figure 3 - DHA: a) System schematic; b) System block diagram.

The actuator position is controlled by an adaptive PI feedback controller and feedforward technique (Figure 3b). The feedforward control action U_a predicts the actuator load to achieve the position reference ($U_a = U_f$). In this work, U_a is resulting from predictive models of the hinge moment and the friction of the actuators. The Feedback controller provides an adaptive control force to eliminate the position error and the gains (K_p and K_i) can be estimated by a recursive system identification process. However, fixed gains ($K_p = 5$, $K_i = 0.25$) were implemented in this paper in order to achieve a similar feedback control system for each topology. The control force signal U_d is defined using a cost function to select the optimal force value. The signal of the selected valves is sent to the delay controller, which is necessary to synchronize the opening and closing of the valves [37]. Since the DHA presents discrete force values, it is necessary to use a locker function. This function avoids the switching of the valves between two consecutive force levels.

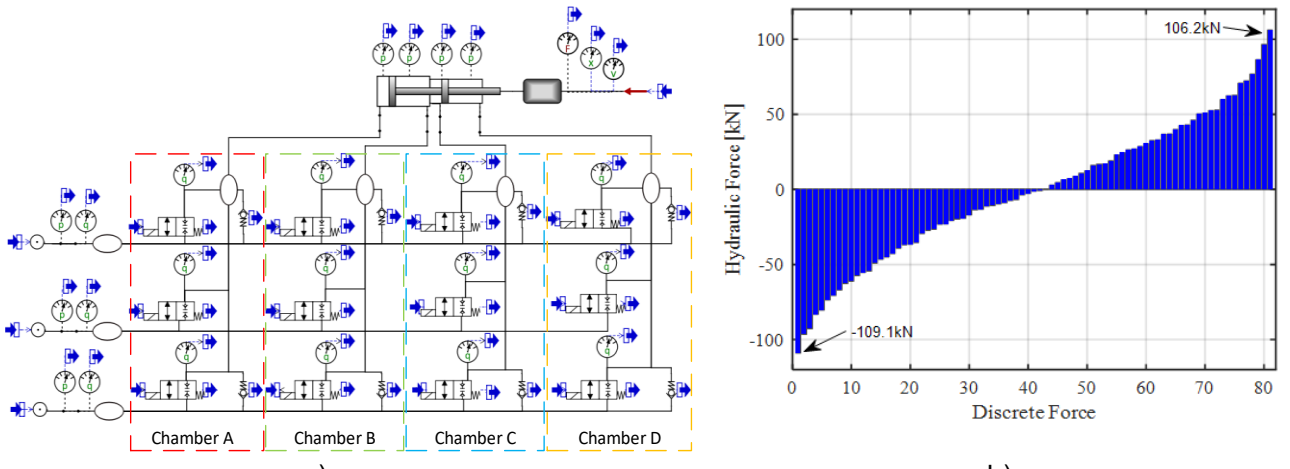

a) b)

Figure 4 - DHA model and force profile: a) Hopsan plant model b) DHA force profile.

A complete description of the sizing process of the DHA to achieve the design requirements is presented in [13]. The areas and pressure lines of the multi-chamber cylinder were sized by the optimization routines described in [6], resulting in the force profile presented in Figure 4b. Each digital hydraulic valve was modeled as a free-leakage 2/2 seat valve with a second-order dynamic behavior. The delay controller parameters were defined according to [37] and the values of the synchronism

times were defined according to the advanced DHA model described in [13]. The defined parameters for the DHA model (Figure 4a) are presented in Table 4.

Table 4 – DHA model parameters [13].

Parameters	Symbol	Value	Unit
Actuator areas	A_A, A_B, A_C, A_D	(22, 27, 17, 13) $\times 10^{-4}$	m²
Chamber death volumes	V_{dN}	1.2×10^{-7}	m³
Actuator leakage	c_{leak}^{Ac}	1×10^{-17}	m³/Pa
Supply pressures	p_{s1}, p_{s2}, p_{s3}	280, 81, 7.5	bar
Valve flow coefficient	k_v	5.3×10^{-8}	m³/sPa$^{1/2}$
Valve open/close bandwidths	$\omega_{n,\,op}; \omega_{n,\,cl}$	1800	rad/s
Valve damping ratio	ξ	0.9	-
Valve solenoid energizing time	t_{on}	2.0	ms
Valve solenoid de-energizing time	t_{off}	4.0	ms
Delay time – on/off valves	t_{ds}	10	ms
Min. time for valve switching	dt_{min}	17	ms

3.2 Digital Electro-Hydrostatic Actuator – DEHA

The Digital Electro-Hydrostatic Actuator (DEHA) (Figure 5a) is another actuator topology developed for aircraft use [8]. However, the DEHA is designed according to the PBW concept, since it includes a decentralized hydraulic power unit, which it gives a great potential to reduce the FCS weight due to the elimination of long and heavy hydraulic lines through the aircraft.

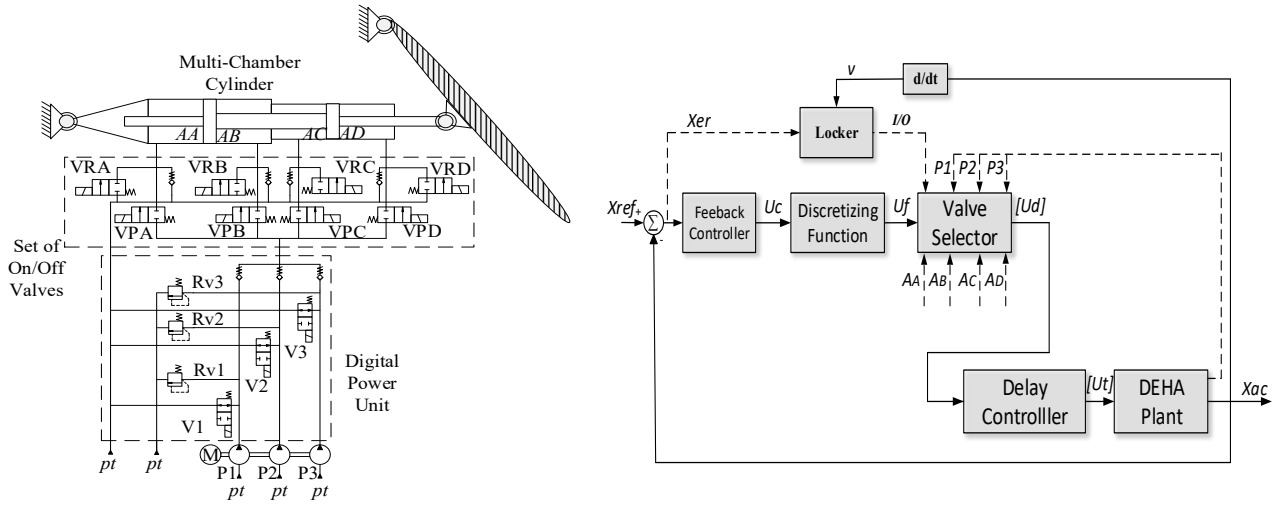

a) b)

Figure 5 – DEHA: a) System schematic b) System block diagram.

A full description of the DEHA is presented in [8]. The DEHA prototype comprises a decentralized digital hydraulic pump (DHP), with 3 fixed displacement pumps coupled at the same shaft and an electric motor with constant speed. With this configuration, it is possible to obtain 8 different volumetric displacements, which are controlled by the first set of 3 free-leakage 2/2 on/off seat valve. Moreover, each section of the DHP presents a relief valve in parallel for safety proposes, and a check valve to prevent pressure peaks and reverse flow from the system to the pumps.

Similar to the DHA, the DEHA secondary conversion unit has a multi-chamber cylinder with different areas and a second set of 8 valves to control the flow rate supplied by the DHP to the chambers of the actuator. Nonetheless, the multi-chamber cylinder combined with this set of valves provides two different operation modes: non-regenerative and regenerative.

In the DEHA forward movement in a non-regenerative mode, the chambers A and C receive flow rate at the same time and the chambers B and D are connected to the reservoir. In the regenerative case, the output flow rate from the chambers B or D can be directed to chambers A and C, resulting in an increasing in the actuator velocity. As a consequence, in the regenerative mode, the DEHA load

capacity is reduced due to the regenerative chamber, which remains pressurized. However, for the non-regenerative mode, the actuator will offer a higher workload capacity with a lower velocity. Therefore, by the combination of the 8 different volumetric displacements from the DHP, and the 6 equivalent areas of the multi-chamber cylinder, the DEHA provides 43 different discrete velocity levels (Figure 6a).

For the DEHA control system, a PI controller is used for the position control (Figure 5b). The output of the PI controller ($K_p = 9$, $K_i = 2$) (U_C) is converted as a velocity signal required for the actuator to achieve the position reference. However, as in DHA, this signal must be discretized in accordance to the velocity profile produced in the DEHA sizing process. Therefore, a cost function was implemented in the discretization function block to set the predefined the velocity output U_f. In this case, the valve combination required to achieve the desired velocity is selected in the valve selector block. The array with the signal of the selected valves [U_d] is sent to the delay controller block to synchronize the valves opening and closing, resulting in the output for the DEHA plant [U_t] [37].

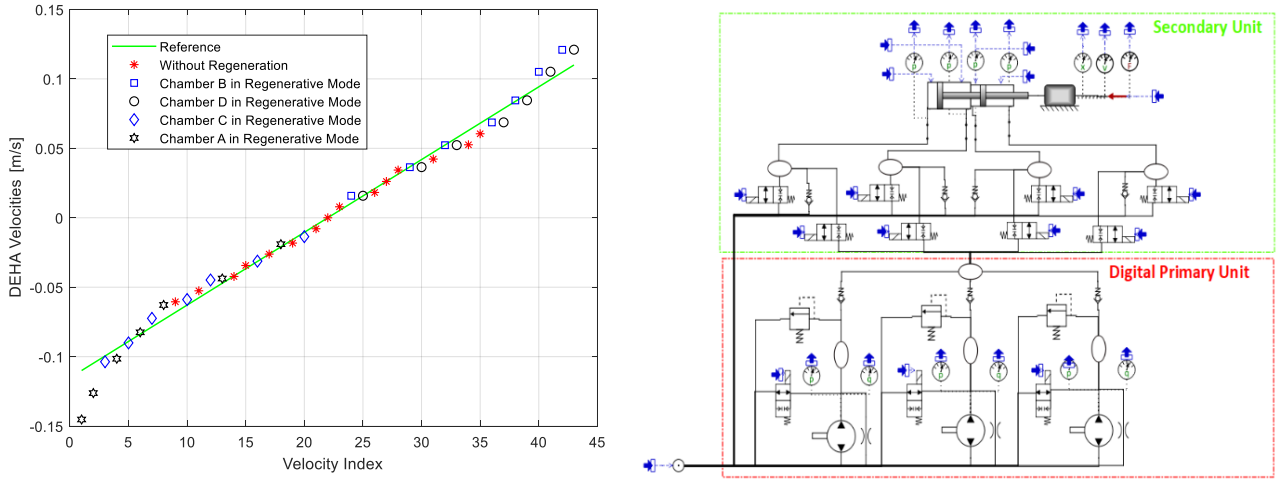

a) b)

Figure 6 - DEHA model and velocity profile: a) DEHA velocity profile b) Hopsan model.

The sizing method based on optimization routines presented in [8] was used to define the parameters for the DEHA model (Figure 6b) in accordance with the design requirements presented in Section 2.2.2. In order to promote the same conditions for a comparative analysis, the models for the on/off valves considering the dynamics of the solenoids used for the DHA were implemented in the DEHA. However, the size of the valves and the delay times were adjusted to offer a better balance between the actuator dynamics and the energy efficiency. Additionally, the locker function was also added with the same aim as described in the DHA. The parameters used in the DEHA model are presented in the Table 5.

Table 5 – DEHA model parameters.

Parameters	Symbol	Value	Unit
Actuator areas	A_A, A_B, A_C, A_D	$(44.19, 37.85, 31.54, 37.88) \times 10^{-4}$	m²
Digital pump displacements	D_1, D_2, D_3	$(2, 4.6, 8.67) \times 10^{-6}$	m³/rev
Digital pump leak. coef.	$c_{leak}^{P1}, c_{leak}^{P2}, c_{leak}^{P3}$	$(4.28, 9.85, 18.12) \times 10^{-13}$	m³/Pa
Digital pump rotational frequency	ω_{DP}	10.472×10^{-2}	rad/s
Primary unit valve flow coef.	$k_{v,p}$	4.6×10^{-7}	$m^3/sPa^{1/2}$
Secondary unit valve flow coef.	$k_{v,s}$	2.1×10^{-7}	$m^3/sPa^{1/2}$
Delay time - Primary unit valves	t_{ds}	5	ms
Delay time - Secondary unit valves	t_{ds}	10	ms
Min. time for valve switching	dt_{min}	20	ms

3.3 Variable Motor Digital Electro-Hydrostatic Actuator – VMDEHA

The third proposed topology is the Variable Motor Digital-Electro-Hydrostatic Actuator – VMDEHA (Figure 7a) [9]. The VMDEHA has significant differences in its operating mode, even though this topology looks similar to DEHA. In this solution, the most significant improvement is the integration of a variable speed electric motor with the digital hydraulic pump to control the actuator, combining characteristics of the digital hydraulics and the Electro-Hydrostatic Actuators (EHAs).

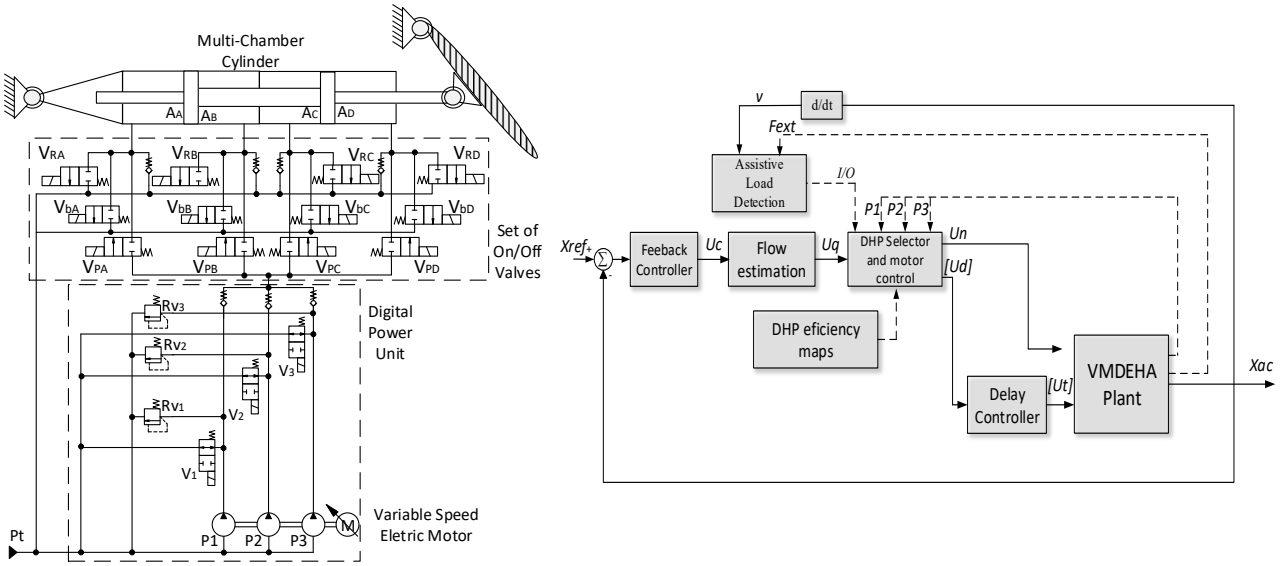

a) b)

Figure 7 - VMDEHA: a) system schematic b) system block diagram.

The variable speed on the electric motor increases the number of flow rate available in the primary conversion unit. In this configuration, the process to design the actuator does not need to develop a strategy to combine the areas of the cylinder, since the regenerative mode is not necessary. Unlike the system with fixed angular speed, where the output flow rate is limited by the number of pumps in the digital pump, the angular speed control is used to achieve the desired output flow rate in the VMDEHA, reducing the effects of the discretized output flow rate. The cylinder movement is controlled by the directional on/off valves, where there is not inversion on the rotation direction of the electric motor. In addition, the on/off valves are used to keep the cylinder position while the pump can be kept running in an idle condition or stopped.

Figure 7a shows hydraulic circuit of the system, which is composed by 1 digital hydraulic pump with 3 fixed volumetric displacement pumps, coupled to an electric motor with variable speed, 15 on/off valves, 3 check valves, 3 relief valves and 1 hydraulic cylinder with four chambers.

The on/off valves in the outlet of the pumps are responsible to direct the flow rate from the pumps to the system or to reservoir. For the four-chamber cylinder, four valves are used to connect the pumps to the chambers (V_{PA}, V_{PB}, V_{PC}, and V_{PD}). Another group of four valves is used to connect each chamber with the return line (V_{RA}, V_{RB}, V_{RC}, and V_{RD}), and the last group is responsible to connect each chamber to the return line when the assistive load is detected by the system, called brake valve (V_{bA}, V_{bB}, V_{bC}, and V_{bD}).

The assistive load occurs when the external load force is in the same direction of the cylinder movement and it can be used for recovering energy. However, the external load in assistive condition accelerates the cylinder, which reduces the system controllability. In order to limit the cylinder speed, when assistive load is detected, only the brake valves are used to connect the chambers to the reservoir. In normal conditions both return valves are used to reduce the flow restriction.

Figure 7b presents the system block diagram, where a position reference is given as an input to the system. For the system control, a PI controller ($K_p = 10$, $K_i = 2$) was implemented. The control signal from the PI controller is converted into a required flow rate, it being the input of the pump combination selector. The DHP selector uses the required flow rate and system pressures to define the pump combination and its angular speed necessary to supply the working conditions. This information is

used to turn on or off the set of valves according to the chosen pumps, cylinder direction and the assistive load. The valve signal is the input signal for a delay controller for synchronizing the opening and closing time of the valves.

The volumetric displacements of the pumps are presented in Table 6 and the flow rates, at a pressure condition of 20 MPa, resulting from the pump combinations are presented in Figure 8b. As it can be seen, a specific flow rate can be supplied by different pump combinations The pump combination selector will choose the combination that results in the best overall efficiency for the required operating point [10].

Table 6 – VMDEHA model parameters.

Parameters	Symbol	Value	Unit
Actuator areas	A_A, A_B, A_C, A_D	27×10^{-4}	m²
Digital pump displacements	D_1, D_2, D_3	$(2, 4, 8)\times10^{-6}$	m³/rev
Primary unit valve flow coef.	$k_{v,p}$	4.59×10^{-7}	$m^3/sPa^{1/2}$
Secondary unit supply valve flow coef.	$k_{v,s}$	1.74×10^{-7}	$m^3/sPa^{1/2}$
Secondary unit return valve. flow coef.	$k_{v,r}$	1.15×10^{-7}	$m^3/sPa^{1/2}$
Secondary unit brake valves flow coef.	$k_{v,b}$	5.81×10^{-8}	$m^3/sPa^{1/2}$
Delay time - Control primary unit valves	t_{ds}	3	ms
Delay time - Control secondary unit valves	t_{ds}	3	ms
Minimum time for valve switching	dt_{min}	5	ms

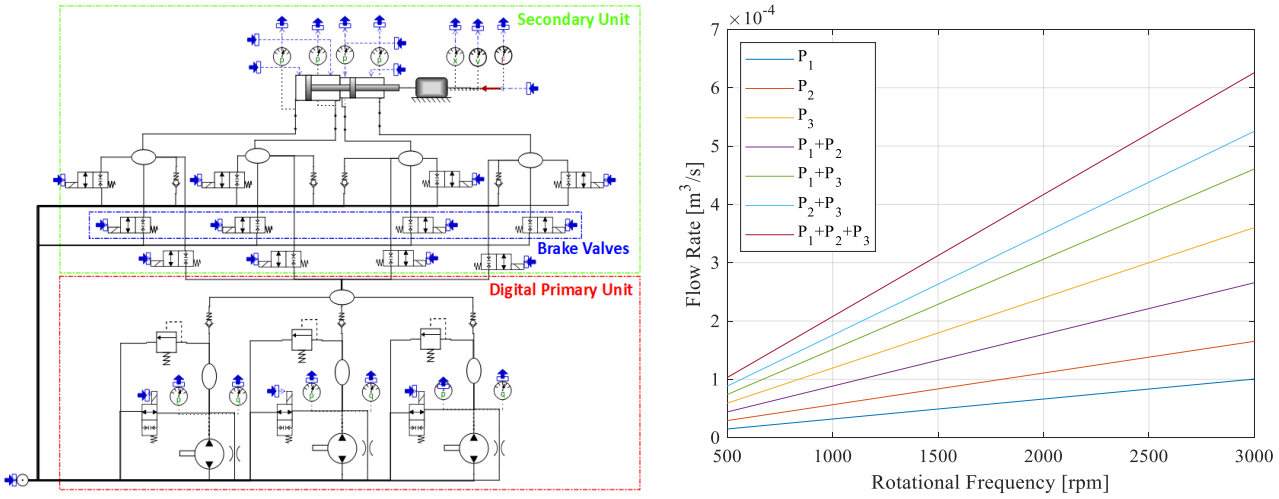

a) b)

Figure 8 - VMDEHA: a) Hopsan model b) Flow rate versus DHP configuration.

4. Results and Discussion

4.1 Proposed Missions

Three different flight missions were considered for evaluating the actuator performances according to their energy consumption and the impact in the GAM flight qualities. Due to the fact that similar effects were observed in the behavior of the actuators and aircraft in the three missions, this paper will focus on demonstrating the key aspects that were examined, highlighting the convergences and divergences in the results of the missions. The initial condition of each mission and the maximum elevon hinge moment produced are presented in Figure 9.

The first aircraft mission was a pure longitudinal maneuver composed by a climb, cruise, and descent flight at 1.2 Mach and 3000 m of initial altitude (red dot in Figure 9), with a duration time of 80 s. The pilot strategy has established as a closed-loop between the pitch inceptor and flight path angle γ, to provide a cruise control (γ = 0) all the time. This control loop is deactivated only to pull and push the pitch inceptor to drive the aircraft. A full pull-down and a full pull-up input in a pilot pitch inceptor

occurred at the simulation time of 10 s and 50 s, respectively, both with 2 s of duration.

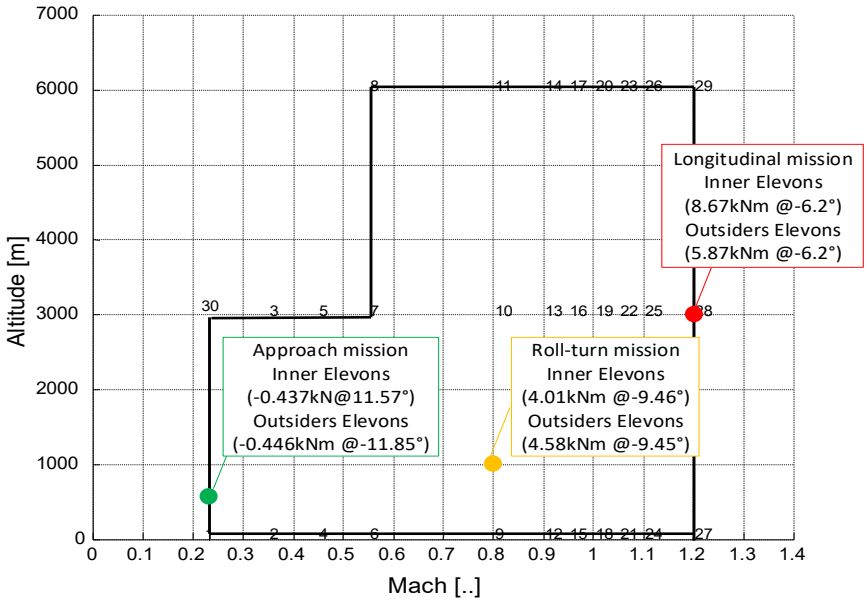

Figure 9 – ADMIRE operating envelope [11] and the mission data.

To evaluate the performance of the aircraft under lateral-directional motion, the second mission consisted of roll and turn maneuvers (yellow dot in Figure 9). The piloting strategy uses a complementary closed loop between the pilot's inceptor and the roll angle (ϕ), defining a roll reference of 90° at 5 s and a full pull-up in the pitch inceptor. In this case, the aircraft describes a turn maneuver ($\psi \approx 45°$), gradually resuming the cruise attitude from the instant 12 s, where the reference angles for the roll ϕ and trajectory γ are set to 0°. The initial conditions for this maneuver were Mach 0.8 and 1000 m, and the simulation duration time was 30 s.

The last proposed mission was an approach maneuver (green dot in Figure 9). The trajectory reference angle γ was adjusted to cause a decedent rate of altitude and lift the nose of the aircraft close to the landing moment to touchdown with the rear landing gears. The initial conditions were defined as Mach 0.2 and 500 m altitude and the leading edge flaps and landing gear engaged. The reference control speed was set to $1.2v_{stall}$ [14].The duration of the mission was defined as 80 s with a slight variation since some configurations of aircraft achieve the mission objective (landing) early.

4.2 Aircraft performance analysis

A more comprehensive analysis can be taken by the evaluation of the aircraft altitude during the described roll-turn mission, since the proposed maneuvers require the FCS efforts from the longitudinal and the lateral-directional controllers. Therefore, this maneuver was selected to show the main points of the interaction between the digital actuators and the ADMIRE FCS. It is important to highlight that no modification was carried out to the FCS (described in [11]) in this work. The ADMIRE aircraft responses are presented in Figure 10.

The flight profiles presented a similar performance in all proposed actuators as it can be noticed in Figure 10a and c. This could be attributed to the similar values achieved for the lateral (φ and ψ) and longitudinal (α and γ) Euler angles, to the slight difference in the roll rate performance, and to the altitude drop at the end of the mission. A slight overshoot of 1.8% can be seen in the roll rate of the ADMIRE equipped with DHA, whereas the VMDEHA and DEHA presented a damped response, similar to the ADMIRE and SHA references, but with an increasing of 0.12 s in response time for the DEHA. During the resumption phase of the cruise flight for the ADMIRE equipped with the digital solutions, oscillations in the longitudinal Euler angles (α and γ) have been observed, with the maximum amplitude deviation of ≈ 0.54° for the DEHA.

Analyzing the pitch rate and load factor during the flight mission, the impact of the digital solutions was most evident. In general, periodic undamped oscillations during steady-state response were observed for the pitch rate and load factor, which are not evident at SHA. In fact, the oscillations of these parameters, in the steady-state, represent an FCS performance degradation for the case of the

ADMIRE equipped with digital solutions. The mean amplitude deviations observed in the digital solutions were 1.42 °/s and 0.41 g for pitch rate and load factor, respectively. Furthermore, the overshoots observed in pitch rate and load factor during the critical interval (7 s to 10 s) should be noted, since exceeding the limits for these parameters may cause higher stress for the aircraft and pilot. In a comparison with the response of the typical ADMIRE configuration, the maximum overshooting deviation values observed for the pitch rate and load factor were -2.55 °/s and -0.24 g for the DHA, 1.64 °/s and 1.03 g for the DEHA, and 0.74 °/s and -0.68 g for the VMDEHA. On the other hand, the SHA presents a damped response compared to the ADMIRE model since a slight reduction in the overshooting was noticed.

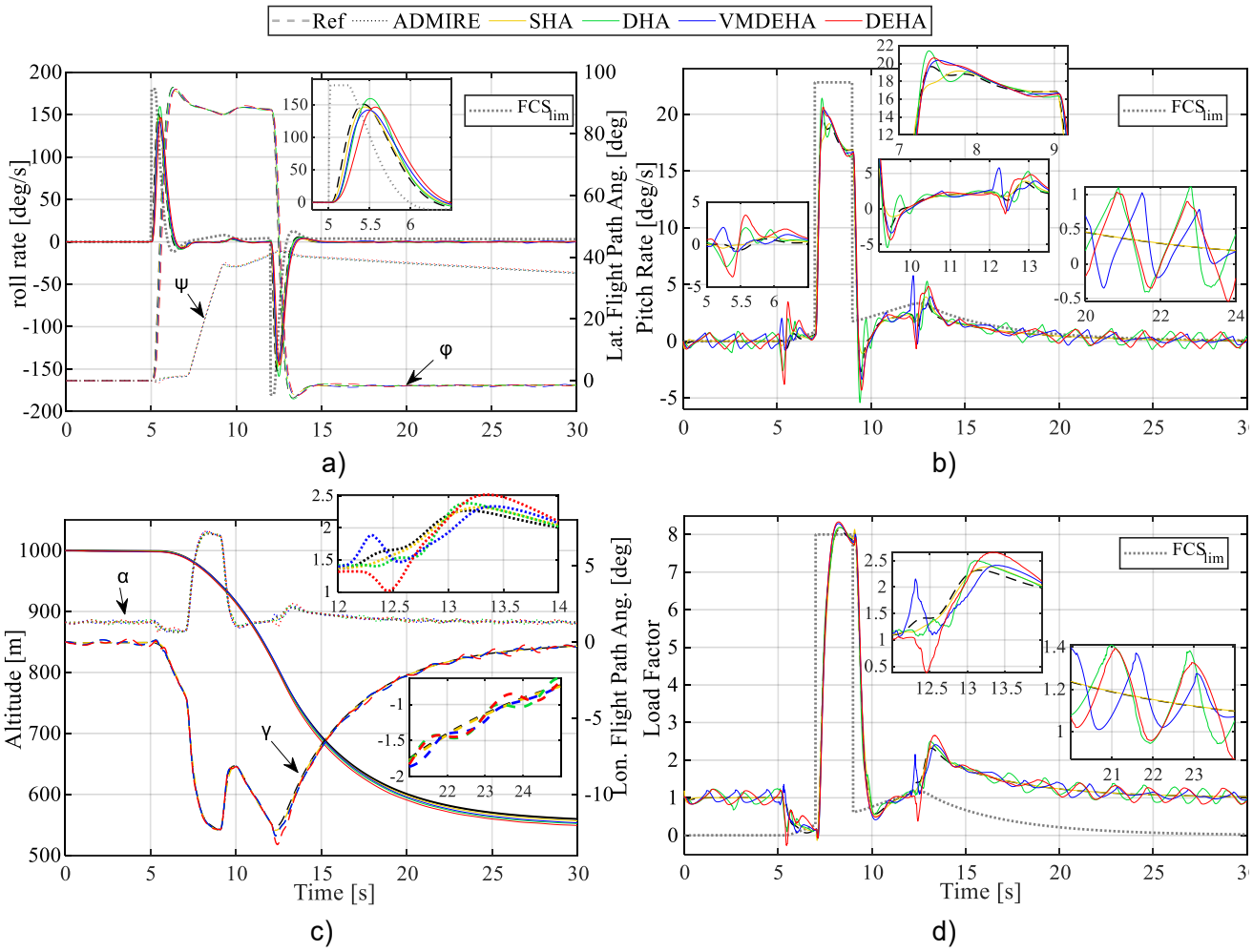

Figure 10 – ADMIRE aircraft responses: a) Roll rate and lateral flight path angles b) Pitch rate, c) Altitude and longitudinal flight path angles d) Load factor.

Although simulations with the digital solutions accomplished the mission with a similar flight profile to the typical ADMIRE configuration, respecting the limits for the FCS controlled states (FCS_{lim}), the effect of these variations should be closely examined in the future to investigate how they affect the flight and handling qualities of the aircraft.

4.3 Actuator performance analysis

This section presents the flight surface performance in the proposed roll-turn mission (Section 4.2.). The surfaces presented are the left inner elevon (LIE) and the left outer elevon (LOE), where the deflections and hinge moments are presented in the Figure 11.

Although all actuators were able to follow the deflection reference (Figure 11a and b), damped oscillations were observed for all proposed solutions. The overshoot values observed between 5 to 5.5 s in Figure 11a are 5.3% for SHA, 13.8% for DHA, 4.8% for DEHA, and 10.9% for VMDEHA, related to ADMIRE reference. Nevertheless, due to the non-linarites and the discretized nature of the digital systems, the dynamic behavior varies according to the type and amplitude of the input signal.

Moreover, the digital actuators presented similar response times for the mission, when compared to

the ADMIRE actuator and the benchmark system SHA. For example, for a displacement of 4.6° (Figure 11a) the values for the actuator response times were 0.168 s for the ADMIRE model, 0.197 s for the SHA, 0.241 s for the DHA and VMDEHA, and 0.351 s for the DEHA.

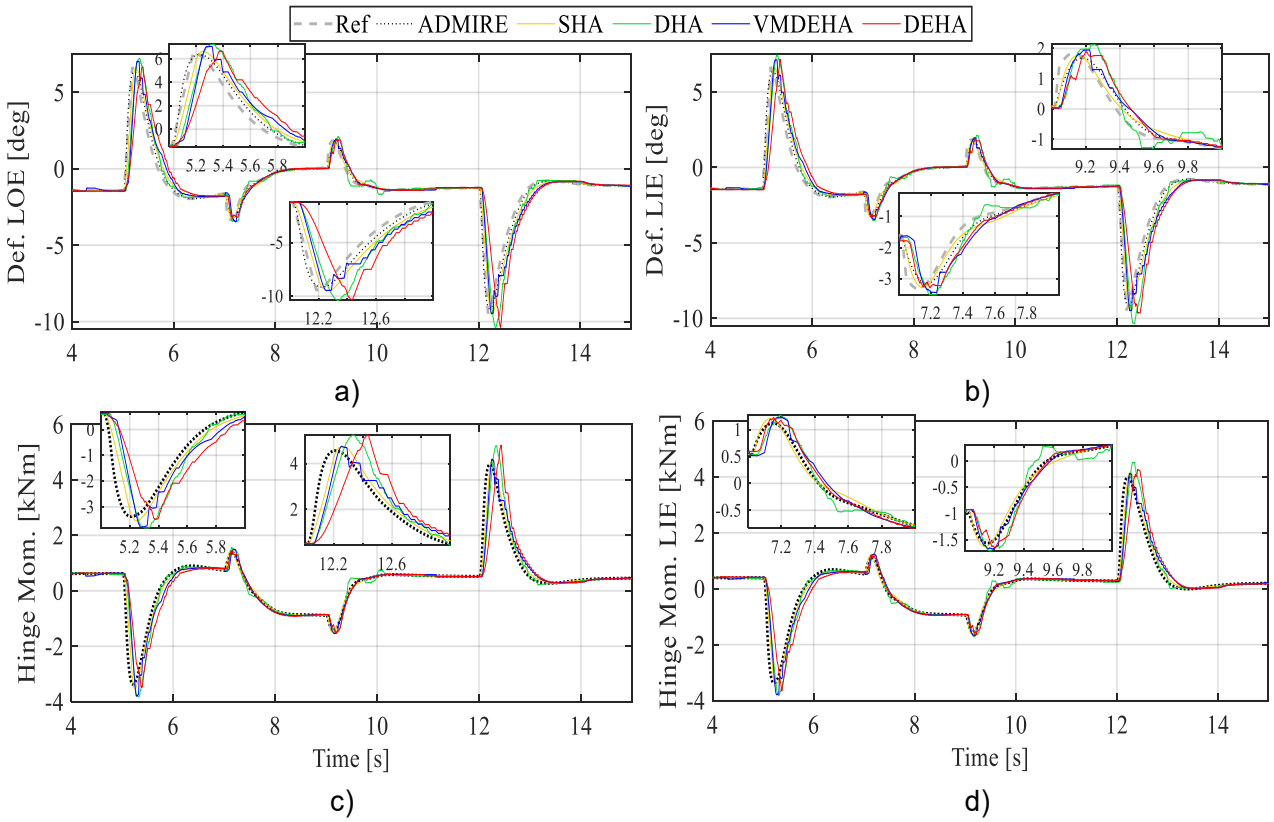

Figure 11 – Flight surfaces response: a) Deflection LOE, b) Deflection LIE, c) Hinge moment LIE d) Hinge moment LOE.

Since similar levels of hinge moment on the flight surfaces were observed (Figure 11c and d), the same output workload was expected for the surfaces. However, greater overshoots and oscillations as described above lead to a higher level of workload on the hydraulic actuators and, consequently, a higher output energy as it will be discussed in next section.

4.4 Energy analyses

Figure 12 presents the input and output energies during the described roll-turn mission for the studied actuation systems. As mentioned above, higher output energy in the digital hydraulic systems compared with a SHA is expected. However, observing the input energy, the benefits of the digital hydraulics are clear. Due to internal leakage in the servovalve of the SHA, the system requires a minimum flow rate to keep it pressurized, demanding supply energy when the control surface is not moving. This justifies the difference in the input energy of 3.75 times when comparing the SHA with DHA in this proposed mission. The energy savings levels are even higher for the proposed hydrostatic topologies where they achieved an input energy savings of 10 and 23 times, respectively, for the DEHA and VMDEHA in a comparison against the SHA.

Figure 13 presents the input and output energies for the three missions through the operating envelope as described in Section 4.1. The input energy in the SHA for all missions are significantly higher than those obtained by the digital solutions (Figure 13 a and d). Otherwise, the output energy in the SHA can be lower or lightly higher than in the digital actuators, depending on the flight control surface displacement and loading (Figure 13 b and e). Consequently, the energy efficiency shown in Figure 13c and f for all missions and the left inner and outer elevons indicates the advantage of the digital hydraulic topologies analyzed in this paper.

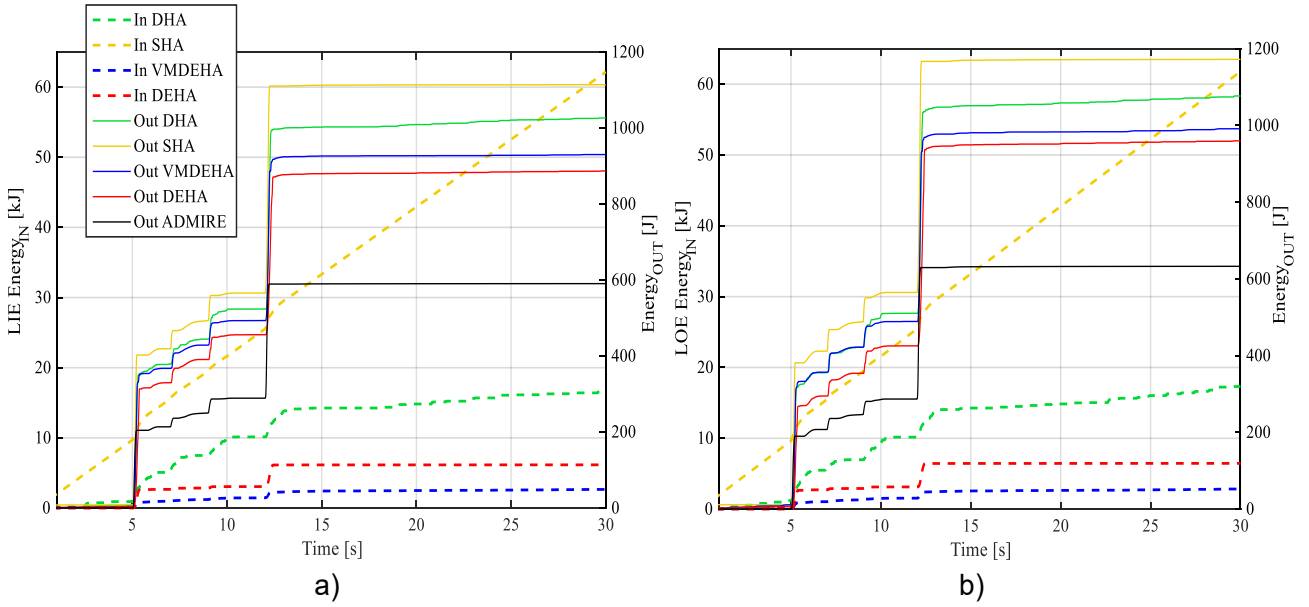

a) b)

Figure 12 – Actuator energies: a) LIE input and output energy, b) LOE input and output Energy.

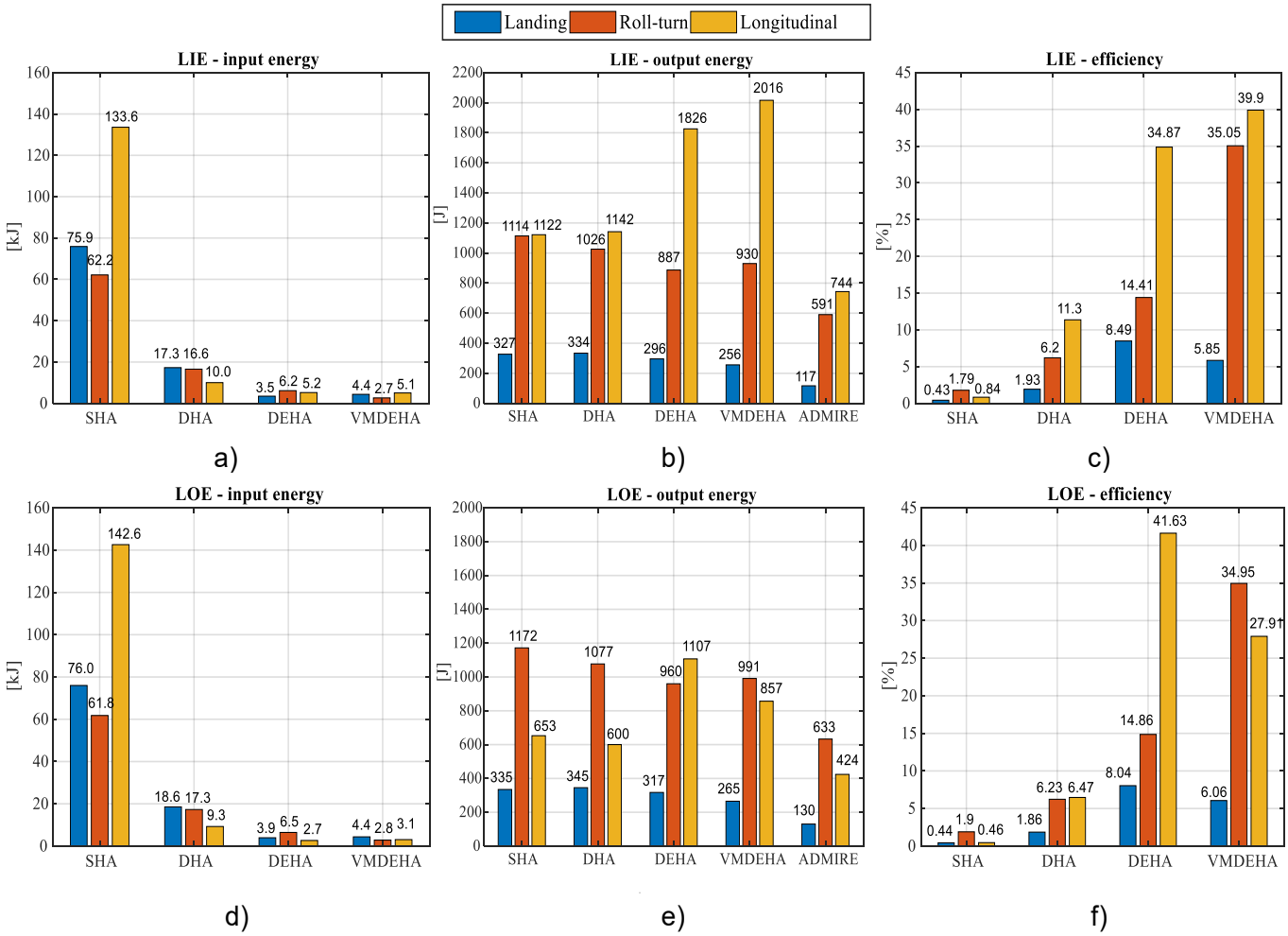

d) e) f)

Figure 13 – LIE and LOE energy consumptions.

The best scenario (SHA vs DEHA LOE in the longitudinal mission) reached an improvement of 52.8 times in the energy savings and 90.5 times in energy efficiency. These high energy savings levels in the DEHA topology are related to the use of a digital pump, where the pump units are kept to the reservoir during the cruise flight, reducing the pump leakages and the output pressure. In addition, a favorable workload scenario for this topology is achieved, which benefits from high amplitude displacements and lower load levels, allowing the strategy of selecting discrete velocities

combinations which utilize the regenerative mode

The results for the DHA are still impressive, reaching an increasing in the input energy savings levels of 13.3 times, which leads an improvement of 13.5 times in the energy efficiency comparing the LIE DHA to SHA in a longitudinal mission. For the LOE at the same maneuver, the DHA performed 15.4 and 14.1 times more input energy savings and efficiency, respectively, when compared to the SHA. However, in the first case, the DHA efficiency values are higher (11.3% against 6.47%), which would support the argument that DHA benefits when there is greater external loading.

Nevertheless, the best average performance among all actuators in terms of energy savings and efficiency is given to the VMDEHA, which obtained an average input energy savings compared to the SHA of 27.3 times, while for the DEHA it was 21.4 times and for DHA it was 6.2 times. This predominance extends to the average efficiency results, where an increase of 26.4 times for VMDEHA, 23.1 times for DEHA, and 6.4 times for DHA were obtained.

5. Conclusions

This paper presented three solutions using digital hydraulic actuators applied to aircraft primary control surfaces. The different topologies were implemented in the ADMIRE, which was used as a virtual platform to simulate different flight missions in order to produce different workload conditions for the actuators. The digital hydraulic solutions were compared with a model of SHA used as a benchmark to evaluate their dynamic response and their energy savings during the aircraft missions. An energy analysis was carried out from a hydraulic system perspective. The analysis shows that the digital hydraulic solutions have a high energy saving potential reaching an average energy saving of 27% allied to a good dynamic response. However, due to nonlinearities and the digital characteristics of the systems, further studies have to be carried out to improve the controllability in some workload conditions.

6. Contact Author Email Address

For any questions, contact the corresponding author by mail: victor.de.negri@ufsc.br.

7. Copyright Statement

References

[1] I. Moir and A. Seabridge, "*Aircraft systems: mechanical, electrical and avionics subsystems integration.*", 3rd ed., vol. 3, no. 2008. Chichester: John Wiley & Sons Ltd, 2008.

[2] H. C. Belan, C. C. Locateli, B. Lantto, K. Petter, and V. J. De Negri, "*Digital Secondary Control Architecture for Aircraft Application*," in The Seventh Workshop on Digital Fluid Power, 2015, pp. 21–39.

[3] J.-C. Maré, "*Aerospace actuators 2: signal-by-wire and power-by-wire.*", London: John Wiley & Sons, Inc., 2017.

[4] V. J. De Negri, P. Wang, A. Plummer, and D. N. Johnston, "*Behavioural prediction of hydraulic step-up switching converters*", Int. J. Fluid Power, vol. 15, no. 1, pp. 1–9, 2014, doi: 10.1080/14399776.2014.882057.

[5] M. Linjama, H. P. Vihtanen, A. Sipola, and M. Vilenius, "*Secondary Controlled Multi-Chamber Hydraulic Cylinder*," in 11th Scandinavian International Conference on Fluid Power - SICFP'09, Linköping, Sweden, 15 pp., 2009.

[6] H. C. Belan, "*Sistemas de atuação hidráulicos digitais para aviões com foco em eficiência energética.* ", Doctoral thesis, Federal University of Santa Catarina, Florianópolis, Brazil, 2018.

[7] D. P. M. Cruz, "*Análise de sistema hidráulico digital para aviões com foco em eficência energética.* ", Master thesis, Federal University of Santa Catarina, Florianópolis, Brazil, 2018.

[8] M. P. Nostrani, "*Development of a digital electro hydrostatic* actuator *for application in aircraft flight control surfaces,*" Doctoral thesis, Federal University of Santa Catarina, Florianópolis, Brazil, 2021.

[9] D. O. Silva, "*Sistema de atuação híbrido para superfícies de controle de aeronaves utilizando bomba hidráulica digital com velocidade variável.* ", Doctoral qualifying dissertation, Federal University of Santa Catarina, Florianópolis, Brazil, 2021.

[10] D. O. Silva, L. A. Carvalho, V. J. De Negri, and G. Waltrich, "*Digital hydraulic pump: an energy efficiency study,*" in Proceedings of the 26th International Congress of Mechanical Engineering - COBEM, p. 10, 2021.

[11] L. Forssell and U. Nilsson, "*ADMIRE The Aero-Data Model In a Research Environment Version 4.0, Model Description*," FOI Report No. FOI-R-1624-SE, December, 2005.

[12] A. Dell'Amico et al., "A *hybrid digital-proportional hydraulic actuation system for aircraft flight control,*" 31st Congress of the International Council of the Aeronautical Sciences, ICAS 2018. Belo Horizonte, 2018. pp. 1-10.

[13] R. S. Jr. Lopes, M. P. Nostrani, L. A. Carvalho, A. Dell'Amico, P. Krus, and V. J. De Negri, "*Modeling and Analysis of a Digital Hydraulic Actuator for Flight Control Surfaces,*" Symposium on Fluid Power and Motion Control FPMC2021. online, October, 2021, doi: 10.1115/FPMC2021-68923.

[14] M. H. Sadraey, *"Aircraft Design: A Systems Engineering Approach"*, 1th ed., vol. 1, no. 2013. New Hampshire: John Wiley & Sons, Ltd., 2012.

[15] S. L. Morris, D. E. Bossert, And W. F. Hallgren, *"Introduction to aircraft flight mechanics."* Reston, USA: Series, AIAA Education, 2003.

[16] USAF, MIL-F-8785C "*Flying qualities of piloted airplanes*." 1980.

[17] USAF, "MIL-F-9490D: "*Military specification flight control systems - design, installation and test of piloted aircfraft, general specification for,*" no. June. p. 97, 1975.

[18] J. L. Townsend and P. E. Blatt, "*New MIL-F-9490D requirements and implications on future flight control design,*" J. Aircr., vol. 13, no. 9, pp. 670–675, 1976, doi: 10.2514/3.58698.

[19] R. S. Jr. Lopes, "*Avaliação do desempenho dinâmico de um atuador hidraulico digital para aplicações aeronauticas em condição de falha.* ", Master thesis, Federal University of Santa Catarina, Florianópolis, Brazil, 2021.

[20] E. Erofeev, A. Skryabin, Steblinkin, and L. Khaletskiy, "*Methodologies and test-rig configurations for experimental improvement of flight control actuation systems,*" Recent Advances in Aerospace Actuation Systems and Components (R3ASC) Conference proceedings, Toulouse, France. pp. 109-116., 2018.

[21] L. Wang, "*Force equalization for active/active redundant actuation system involving servo-hydraulic and electro-mechanical technologies*," Doctoral Thesis, Université de Toulouse, Toulouse, France. 2012.

[22] S. Wang, M. Tomovic, and H. Liu, *"Commercial aircraft hydraulic systems.*" Waltham: Elsevier Inc., 2016.

[23] P. Krus, R. Braun, P. Nordin, And B. Eriksson, "*Aircraft System Simulation for Preliminary Design.,*" 28th Congress of the International Council of the Aeronautical Sciences, ICAS 2012, Brisbane, Australia, 2012.

[24] J.C. Maré, "*Aerospace actuators 1: needs, reliability and hydraulic power solutions.*" London: John Wiley & Sons, Inc., 2016.

[25] G. E. Tagge, L. A. Irish, and A. R. Bailey, "S*ystems Study for an Integrated Digital/Electric Aircraft (IDEA),*" NASA Contractor Report 3840, 1985, p. 206.

[26] A. W. Waterman, "*The boeing 767 hydraulic system,*" SAE Transactions Vol. 92, Section 4: 831406-831830, 1984. https://www.jstor.org/stable/44647773%0A (accessed Apr. 13, 2021).

[27] K. Thompson, "*Notes on 'the electric control of large aeroplanes,'*" IEEE AES Magazine, Lockheed - Georgia Company, Marietta, Georgia, pp. 19–24, 1988.

[28] R. Navarro, "*Performance of an electro-hydrostatic actuator on the F-18 systems research aircraft,*" NASA Tech. Memo., no. 206224, 1997.

[29] I. T. Raymond and C. W. Robinson, "*Aircraft digital input controlled hydraulic actuation and control system,*" in Boeing Military Airplane Company, 1981, p. 220.

[30] Y. Lin, E. Baumann, D. M. Bose, R. Beck, and G. D. Jenney, "*Tests and techniques for characterizing and modeling X-43A electromechanical actuators,*" no. December, 2008.

[31] G. Di Rito, E. Denti, and R. Galatolo, "*Development and experimental validation of real-time executable models of primary fly-by-wire actuators*," Proc. Inst. Mech. Eng. Part I J. Syst. Control Eng., vol. 222, no. 6, pp. 523–542, 2008, doi: 10.1243/09596518JSCE546.

[32] G. Di Rito and R. Galatolo, "E*xperimental assessment of the dynamic stiffness of a fault-tolerant fly-by-wire hydraulic actuator*," Proc. Inst. Mech. Eng. Part G J. Aerosp. Eng., vol. 226, no. 6, pp. 679–690, 2012, doi: 10.1177/0954410011413986.

[33] N. E. Wood and R. A. Lewis, "*Electromechanical actuation development,*" in Research Manufacturing Company of California, 1978, p. 412.

[34] H. Backström and E. Kullberg, "*Report on the usage of the Generic Aerodata Model,*" 1996.

[35] A. D. C. de DE NEGRI, V. J., RAMOS FILHO, J. R. B., SOUZA, "Design method for hydraulic positioning systems.", 51th National Conference on Fluid Power (NCFP), Las Vegas, USA. pp. 669-679 2008.

[36] R. BRAUN and P. Krus, *"Tool-Independent distributed simulations using transmission line elements and the functional mock-up interface.",* 54rd SIMS conference on Simulation and Modelling, Bergen, Norway, 2013.

[37] I. J. Mantovani, H. A. Kagueiama, A. T. de C. Gama, A. Dell'Amico, P. Krus, and V. De Negri, *"On/off valves synchronization and reliability evaluation of a digital hydraulic actuator."*, Symposium on Fluid Power and Motion Control FPMC2020. Bath, UK, p. V001T01A041., 2020.